*Article*

# Electron mean free path effect on vortex matter in a superconducting Pb island grown on Si (111)

**Jesús González [1]*, Jader González [2], Fernando Durán [2], Carlos Salas [1], and Jorge Gómez [1]**

[1] Universidad del Magdalena; Carrera 32 No 22 – 08 Santa Marta D.T.C.H. - Colombia, Postal Code No. 470004
[2] Universidad Pontificia Bolivariana-Bucaramanga; Autopista Piedecuesta Kilómetro 7, Floridablanca, Santander- Colombia, Postal Code No.681004
* Correspondence: jgonzaleza@unimagdalena.edu.co

**Abstract:** In this work we report recent theoretical calculations of a superconducting island in a strong vortex confinement regime. The obtained results reveal the evolution of superconducting condensate as a function of electron mean-free path ($l$) with the evolution of an applied magnetic field $H_0$. The results of this study provide an insight about the emergent superconducting properties under such conditions, using the Ginzburg-Landau numerical simulations where spatial variation of thickness $d$ on island, omnipresent in these kind of structures grown on Si (111), is taken into account. These results offer a new route to tailor superconducting circuits by using the controlled bombardment, in order to explore the impact on vortex distribution, phase of order parameter, number of vortices, free energy and the first $H_1$ and second critical field $H_2$.

**Keywords:** strong vortex confinement; superconductivity; Ginzburg-Landau theory; superconducting island; free energy

## 0. Introduction

Superconductivity is an electronic state of matter characterized by specific length scales: the coherence length $\xi$, the length scale of the Cooper-paired electrons, and the London penetration length $\lambda$, the length scale of magnetic field penetration into the superconductor [1]. The superconducting state is attained below certain critical values of temperature, magnetic field, vortex structures and applied current, which can change dramatically when the size of a superconductor becomes comparable with the characteristic lengths [9–11]. In this state, the resistance to the passage of an electric current exhibited by the material is zero [12]. In past decades several theoretical studies focused on the confinement effects in superconductors of a size lower than one or both of these characteristic scales [2–4], but also, focused on the effect of symmetry on condensate confinement comparing mesoscopic disks, squares and triangles [5–8]. The theoretical macroscopic framework that built upon the definition of a superconducting wavefunction that characterizes the superconducting state, comes from the Ginzburg–Landau theory [2] which is used in this work.

Most experimental focused on measuring the overall response of previous mentioned systems and superconducting islands [13–18], or to the local study of the magnetic confinement of vortices considering low magnetizing field $H \lll H_{c2}$ on large samples $d \sim \lambda \ggg \xi$ [19,20]. The vortex configuration in real space at high fields $H \ggg H_{c1}$ was studied in [16], but low confinement conditions are still considered, $d \ggg \xi$. Nowadays, penetration and expulsion of vortices in mesoscopics superconducting samples has been studied in Ref. [21–24], but the detailed picture of a strongly confined superconducting state $d \sim \xi \lll \lambda_{eff}$ is still missing, including the influence of changing electron mean free path $l$ , not only experimentally but also theoretically.

There are two effective techniques for modifying the mean free path of the electron $l$, such Focused Ion Beam Induced Deposition (FIBID) and Focused Electron Beam Induced Deposition (FEBID), which are two very similar nanopatterning techniques that use of a focused beam of charged particles, either ions or electrons [25–27]. In general, irradiation-induced doping or disorder exhibits higher accuracy compared to others such as substitutional chemestry, in which there are greater uncertainties and inhomogeneity in



**Citation:** González, J. D.; González, J. E.; Durán, F.; Salas, C. M.; Gómez, J. Electron mean free path effect on vortex matter in a superconducting Pb island grown on Si (111). *Preprints* **2023**, *1*, 0. https://doi.org/

Preprints (www.preprints.org) | NOT PEER-REVIEWED | Posted: 13 June 2023 doi:10.20944/preprints202306.0911.v1



phase distribution in the induced disorder [28,29]. Irradiation of superconductors generally leads to a significant increase in the normal-state resistivity and suppression of $Tc$, as well as an enhancement of the critical current density when efficient pinning centers are created [30].

This has driven nanofabrication techniques because there is a perennial need for both industry and research to exploit such fundamental effects for the development of quantum technologies [31], in which superconducting nanodevices represent a field of research. Such devices include magnetic sensors in the form of superconducting interference superconducting quantum interference devices (SQUIDs) [32], single-photonic detectors [33], quantum bits [34] and quantum switches [35].

## 1. Materials and Methods

We simulated a superconducting Pb island grown on a silicon substrate (111) as illustrated in Fig. 1, but also, the thickness change $d$ and the mean free path $l_e$. The framework for our theoretical studies is the phenomenological Ginzburg-Landau (GL) theory [1]. We used the expressions for GL coeficients $\alpha$ and $\beta$ in the dirty limit, to include the variation $l_e$ the electron mean free path in the sample, i.e.

$$\alpha(T) = -1.36\frac{\hbar}{2m^*\xi_0 l_\xi}\left(1-\frac{T}{T_c}\right) = \frac{\alpha_0}{l_{\xi_0}}\left(1-\frac{T}{T_c}\right) \quad (1)$$

$$\beta = \frac{0.2}{N(0)}\left(\frac{\hbar^2}{2m^*\xi_0 l_e k_B T_c}\right)^2 = \frac{\beta_0}{l^2_{\xi_0}} \quad (2)$$

Where $l_\xi = \frac{l_e}{\xi_0}$ is the ratio of the electron mean free path and BCS coherence length. The dimensionless form of the GL equations can be written as follow:

$$(-i\nabla - \mathbf{A})^2\Psi = \left(\frac{1.367}{l_{\xi_0}} - \frac{1}{l^2_{\xi_0}}|\Psi|^2\right)\Psi \quad (3)$$

Where lengths are scaled to $\xi_0$, penetration depth $\lambda_0$ is defined as $\lambda_0^2 = mc^2\beta_0/16\pi|a_0|e^2$, the vector potential $\mathbf{A}$ is expressed $\phi_0/2\pi\xi_0$, and the order parameter is in units of $\Psi_0 = \sqrt{-\alpha/\beta}$.

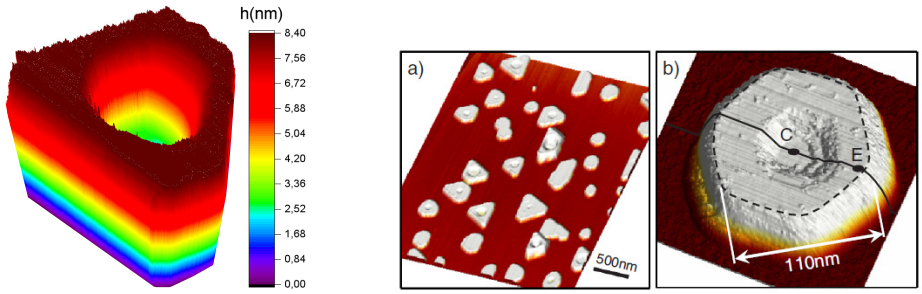


**Figure 1.** (Color online) (Left) Computational simulation: Pb superconducting island using data extracted from the experiment, which gives greater precision to the results obtained. (Rigth) Experimental results: Scanning tunneling microscopy (STM) images of Pb islands on Si(111) surface taken on a large scale (a) and on a local scale (b) showing locations C and E correspond, respectively, to the island center and edge [21]. The effective diameter of the studied Pb island was estimated as $D_{eff} \approx 3.6nm$ and its thickness in the border as $d \approx 8.4nm$ whereas inside the island hole $d_{int} \approx 2.52nm$, corresponding to 2–3 single atomic layers of Pb in (111) direction.

Preprints (www.preprints.org) | NOT PEER-REVIEWED | Posted: 13 June 2023 doi:10.20944/preprints202306.0911.v1



## 2. Results and discussion

Process started calculating the full free-energy ($F$) spectrum and the corresponding vortex states as a function of applied magnetic field ($H_0$) for the island with a central hole and $l_\xi = 1.0$ Fig. 2. Initially, the magnetic field was kept perpendicular to the plane bottom of Pb island. The method for finding vortex states is multifold: First step, applied magnetic field is increased and decreased in the considered range with a kept history of the previously found states in the field sweep and the second step, considering each value of magnetic field, the calculation is initialize from the fluctuating normal state (randomized $|\Psi| < 0.01$) and from the from the fully superconducting state ($|\Psi| \approx 1$). Following this steps, we construct the energy diagram of all stable vortex states, including those with higher energy. As a result, we found more than one stable vortex distribution, i.e. one with lowest energy (ground state) and several others with higher energy (usually called metastable).

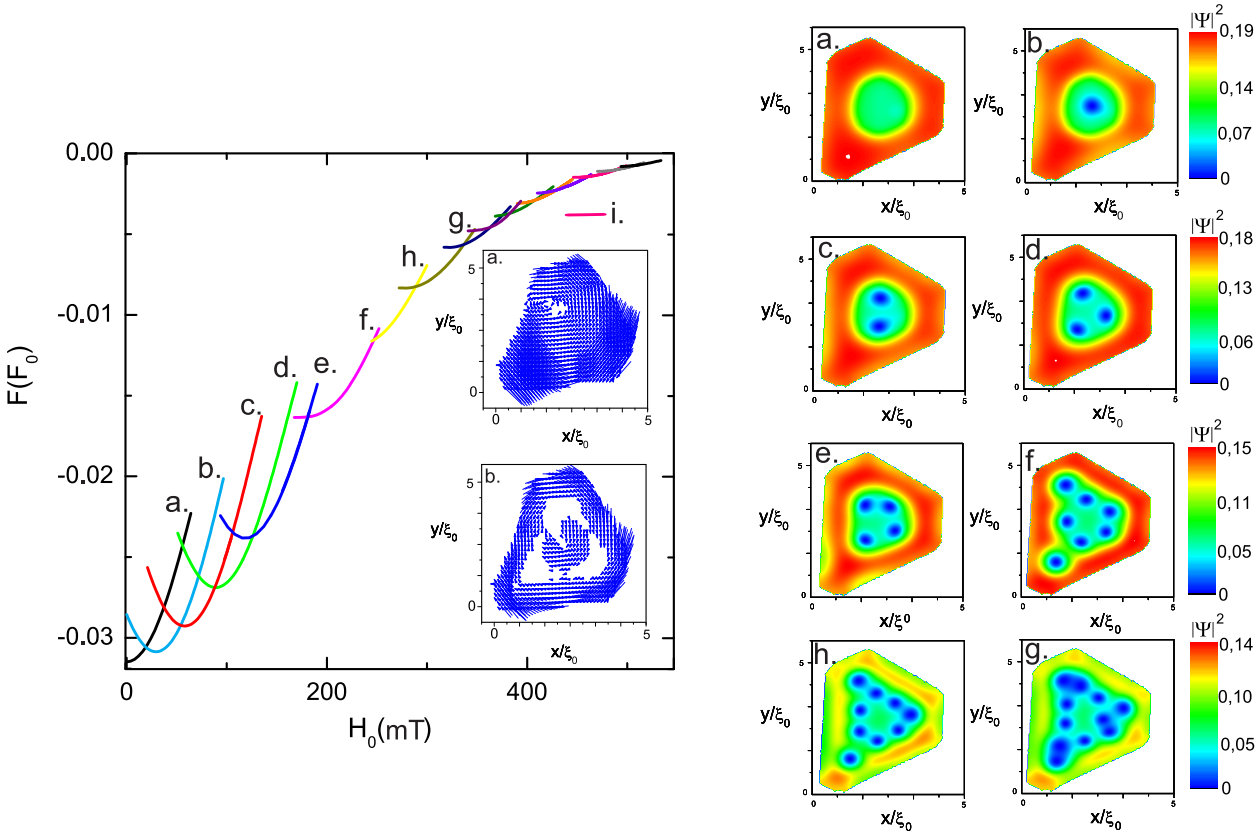


**Figure 2.** (Color online) (left) Free-energy curves and corresponding vortex states in a Pb island with one central hole, in a magnetic field perpendicular to the sample. The insets show the superconducting current for selected cases. (Right) Contour plots of the Cooper-pair density for selected different vortex states, the color bar of the islands snapshot evolves from red to blue, reflecting the reduction of the condensate strength.

We show lower energies and a higher stabilities represented in the wide ranges of magnetic fields in which the same number of vortices remains (see Fig. 2, cases a.,b.,c.,d. and e.). This finding demonstrates the strong confinement imposed on vortices by Meissner currents on the edge of the island (see Fig. 1), where the Meissner current is strongest, as we can notice in the snapshots of superconducting current (see Fig. 2 (left) inset) and it confines vortices toward the interior of the sample. On the other hand, It can also be noted that stability decreases with the entry of a greater number of vortices when the magnetic field is increasing (see Fig. 2, cases f.,h. and g.), due to vortices are basically parallel magnetic moments that destroy the superconductivity with increase of their number. Additionally,

Preprints (www.preprints.org) | NOT PEER-REVIEWED | Posted: 13 June 2023 doi:10.20944/preprints202306.0911.v1



other evidence of the strong confinement on the superconducting island can be noticed that vortices repel each other, and this repulsion, in the absence of sample boundaries, leads to the formation of a triangular (Abrikosov) lattice, which is not the case in this research.

Fig.3 (a), (b), (c), (d) inset show some states where vortices have reached the center of superconductor island which can be verified by the circular diagram phase of the order parameter on the top of the island simulation. The vortex state is characterized by the total angular momentum $L$ through $\Psi = \psi exp(iL\phi)$, but, we can introduce an analog to the total angular momentum which is still a good quantum number. Choosing circular loops at the periphery of the center of the island, we find that the effective angular momentum $L = \Delta\phi/2\pi$, and each time that in the path the color went from red to blue a vortex is found $L = 1, 2, 3, ....$ The superconducting order parameter $|\Psi|$, nucleated at the sample surface, traps then inside, in the island hole, carrying flux $L\phi_0$ where $\phi_0$ is the quantum flux . To check this "flux compression" model quantitatively, the self-consistent solution of the full Ginzburg-Landau (GL) equations is necessary Eq.3

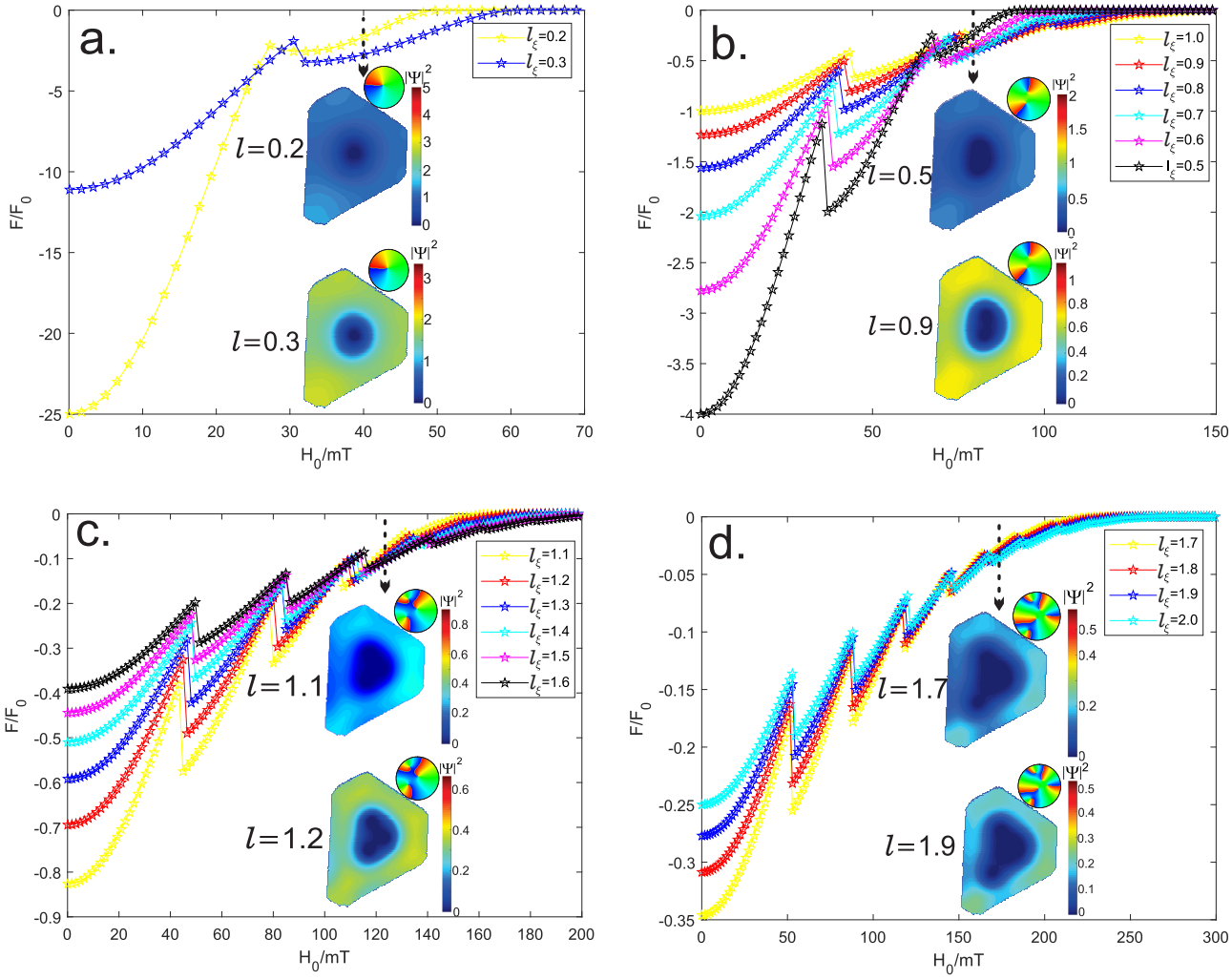


**Figure 3.** (Color online) Free-energy curves for island with different values of $l$ as a function of applied magnetic field perpendicular to the sample. Insets show the Intersection of the sections of curves representing the state without vortices and the first vortex entry, representing the first critical field $H_1$.

The transition between the two quantum states $L = 0$ (zero vortex) and $L = 1$ (one vortex) can be used to calculate the field $H_1$, corresponding to the penetration of the first flux line into a superconducting island. One option to find the value of $H_0$ in which this

Preprints (www.preprints.org) | NOT PEER-REVIEWED | Posted: 13 June 2023 doi:10.20944/preprints202306.0911.v1



transitions take place is considering every curve of Fig. 3 (a), (b), (c) and (d) where the peaks obtained at a lower value of applied magnetic fields in every curve of Fig. 3 ($F$ versus $H_0$), represent the first vortex entrance in the superconducting island, we can notice that it take place at different values of $H_0$. Fig. 3 also can be used to calculate the field $H_0$ corresponding to the penetration of one flux line at different electron mean-free path $l_\xi$, and thus the transition between the two quantum states $L = 0$ and $L = 1$, as well as by using $l$ we can tune the number of peaks or transitions.

The characteristics lengths of a superconductor, the coherence length and the penetration depth, take the effective values $\lambda_{eff} = 0.65\lambda_0\sqrt{\xi_0/l}$ and $\xi_{eff} = 0.85\sqrt{l\xi_0}$ considering $l_\xi = l_0/\xi_0$. Thus, the situation in the island is similar to that of a type II superconductor in the diffusive limit, in which correlation length $\xi$ and penetration depth $\lambda$ in a magnetic field depends on $l^{0.5}$ and $l^{-0.5}$ respectively. Therefore, the magnetic field in a superconductor is affected due to the increment of $\lambda$ with the increases of concentration of impurities, but also a strong variation of the number of superconducting electrons, i.e. electrons linked in Cooper pairs with the decrease of $\xi$. This behaviour is shown in Fig. 2 and Fig 3. (inset) where variations of condensate are reached considering a spatial change of the electron mean free path.

In addition, the order parameter $|\Psi_0|^2$ is modified through the sample with the modification of $l$, as we expected, according to the proportionality between the order parameter and penetration depth which is $|\Psi_0|^2 \sim 1/\lambda$. It implies changes on strong screening supercurrents (see Fig. 2 inset) that may circulate in the island, where strong supercurrent carry on a strong diamagnetic (Meissner) effect as we can notice in Fig. 3 where the $H_1$ (first vortex entry) is reached (see also table A1 apendix A). It also can be noticed in the modification of $l$ at different zones of sample (see Fig. A1 apendix B) which allow to chose not only the location of vortex entrance, but also, the value of $H_0$.

Fig. 4 (left) shows the proportionality of the green curve corresponding to the values of the second critical magnetic field where the normal state is reached ($H_2$) versus the mean free path ($l$), which shows a result not reported before for this type of heterostructures. The fine tune of $H_2$ shows great applications for the design of electronic devices, through the bombardment of the Pb islands, which can be controlled using high precision with current technologies. Thus, it is clear that $H_1$ can be tuned, which supposes a variation in the Meissner current and with it the repulsion of the applied magnetic field $H_0$ and entry of vortices in the superconducting island. We know that flux penetration in type-II superconductors occurs in form of quantized, flux-enclosing, supercurrent vortices. However, a more detailed analysis shows that, this flux penetration must first overcome an energy barrier at the surface which is called Bean-Livinstong barrier (BLB). Corresponding variations of the Gibbs free energy with $l$, for several values of $H_0$, are shown in Fig. 3. One can see that $H_1$ take different values due to, in order to penetrate the superconductor island, vortex must first overcome BLB.

In order to identify the observed quantum phenomenon, we explored the evolution and stability of the superconductivity in the islands with the magnetic field (Fig. 2, 3 and 4). At zero magnetic field, Fig. 2 snapshot (a.) shows a spatially homogeneous superconducting condensate to exist in the entire nanoisland, evidencing the Meissner ($L = 0$) state. As the field increases further, the snapshots in Fig. 2 and 3 reveal novel intriguing vortex configurations, evolving till the normal state is achieved in each the superconducting island, but in order to get a deeper insight into the field evolution of the condensate confined we need to focus on their phases.

Preprints (www.preprints.org) | NOT PEER-REVIEWED | Posted: 13 June 2023 doi:10.20944/preprints202306.0911.v1



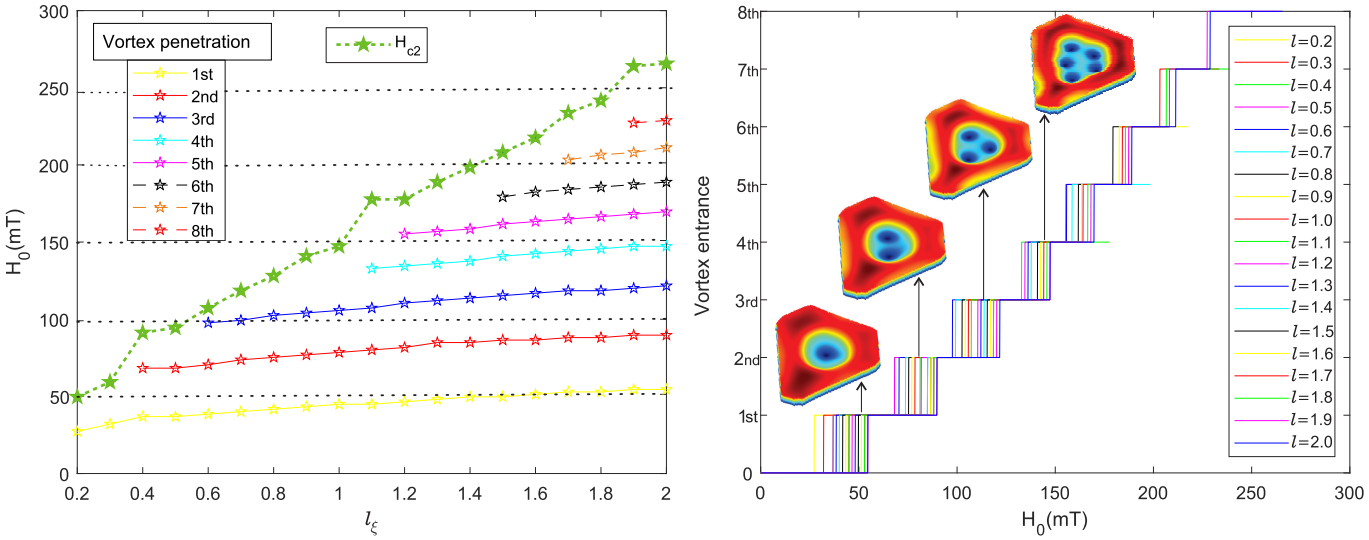


**Figure 4.** (Color online) (Left) Values of the applied magnetic field $H_0$ versus electron mean free path $l$, the green curve shows the values of the second critical magnetic field $H_2$ reached for each value of $l$ selected, evidencing the direct proportionality between both magnitudes. While the yellow curve shows the values of $H_0$ for which the Bean-Livistong barrier (BLB) [36] is exceeded $H_1$ (first critical field) or first entry of vortices, whose inclination from $l = 0.2$ to $l = 2.0$ of the BLB because in the first case the sample is in the dirty limit ($l \ll \xi$), while in the second case it is in the clean limit ($l \gg \xi$). (Right) Entry of vortices in the sample as a function of $H_0$, inset some configurations of vortices that show that up to approximate values of $H_0 = 150mT$ the vortices penetrate one by one. Each line in this graph has a correspondence in fig. 3, where each jump in the Gibbs free energy curve evidences the entry of vortices.

In Fig. 5 we present a color-coded diagram of (ZBC) vs magnetic field taken over a line crossing the island (depicted as a black line in the blue frame). This diagram shows a series of abrupt steplike transitions which are identified in a separating the states with different vorticity $L$, where color from red (superconducting state) to blue (normal state) corresponds to the local strength of superconducting condensate. Precisely, until $H_0 \approx 27.5mT$ the island remain in the Meissner state ($L = 0$) for $l = 0.2$, in agreement with the color map in Fig. 5. Also, we can notice that only one vortex penetrate due to only one steplike transition take place for $l = 0.2$ until reach the total normal state at $H_0 \approx 46.49mT$ (all region became blue). In order to get a deeper insight into these phases, we focused on the field evolution of the condensate confined in the superconducting island with $l = 1.2$. At $H_0 \approx 46.49mT$ T the first vortex appears in the sample; it is clearly identified by its normal state core (blue region). This single vortex state lasts until $H_0 \approx 78.49mT$. The $L = 2$ phase occurs at $H_0 \approx 78.49mT < H_0 < H_0 \approx 110.49mT$, followed by the $L = 3$ state, that also can be noticed in the CPD in the red snapshot located up of the $H_0 \approx 110.49mT < H_0 < H_0 \approx 134.49mT$.

Preprints (www.preprints.org) | NOT PEER-REVIEWED | Posted: 13 June 2023 doi:10.20944/preprints202306.0911.v1



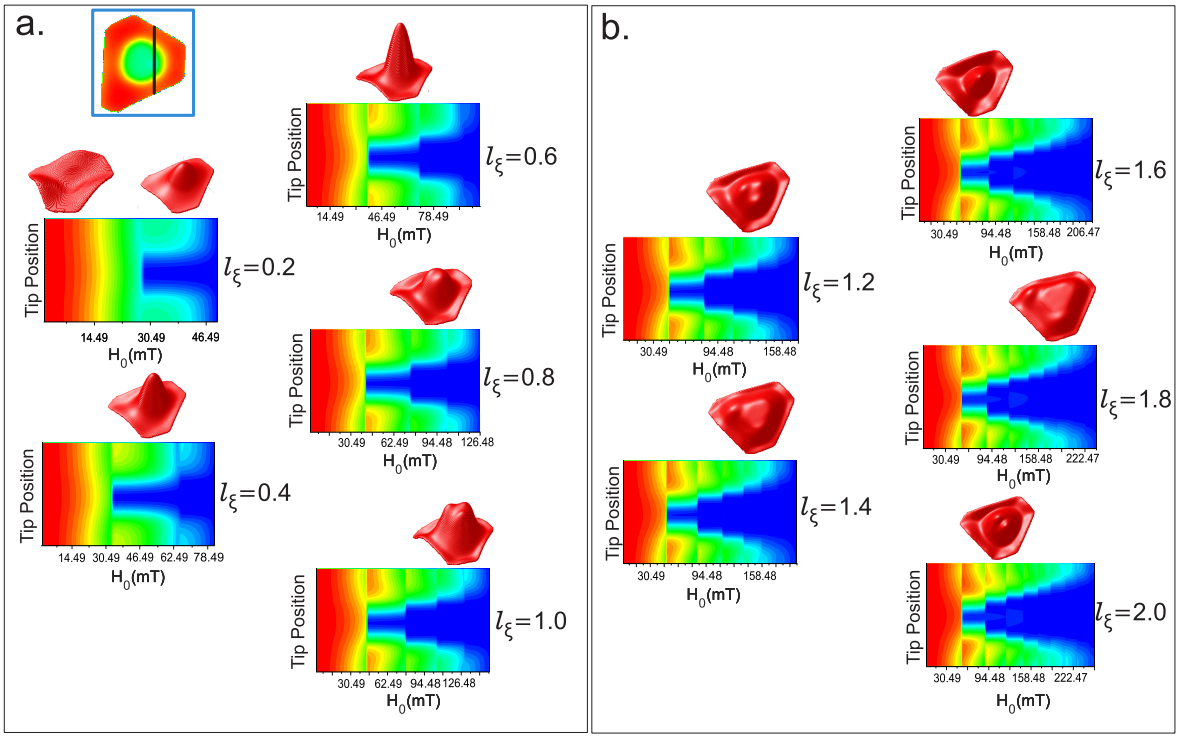


**Figure 5.** (Color online) (a,b) Phase diagrams of the value of Cooper-pair density (CPD) under the tip as a function of magnetic field, obtained as the tip is moved along the line that runs through the island, and taken during sweep up and down of the magnetic field. The corresponding spatial distribution of CDP (red shapshot) for selected steplike transitions where every peak correspond to vortex position in the island. Black line on figure inside blue frame indicates the trajectory over which the tip was moved in order to simulate the scanning tunneling microscope (STM) to obtain the zerobias conductance (ZBC) phase diagram.

Remarkably, in $L = 2$ for $l = 0.8$ looks like a single round object located at the island center, instead of two individual vortices. The straightforward conclusion is that here one (two) individual vortex cores are merged to form a single giant vortex.

## 3. Conclusions

In conclusion, strong vortex confinement effects were studied in Pb island grown on Si (111), taking into account several changes of electron mean-free path, considering that experimentally to ion bombardment can be done over a superconducting sample, by using the expressions for Ginzburg-Landau (GL) coefficients $\alpha$ and $\beta$ in the dirty limit. In these type II superconducting island an unexpected behaviour of vortex configuration was studied, but also, their critical parameters which allow to control this heteroestructure in order to be applied in electronic devices.

**Author Contributions:** Derived G-L equations for dirty limit and performed the simulations, J.D. González and J.E. González; prepared the figures, F. Durán and C. Salas; software, J.D. González; formal analysis,J.D. González and J.E. González; writing original draft preparation, J. Gómez and J.D. González.

**Acknowledgments:** This work was partially financed by the Universidad del Magdalena (Fonciencias) and Dirección de Investigación (Colombia) y Transferencia (DIT) Universidad Pontificia Bolivariana (Colombia).

**Conflicts of Interest:** The authors declare no conflict of interest. The founding sponsors had no role in the design of the study; in the collection, analyses, or interpretation of data; in the writing of the manuscript, and in the decision to publish the results.

 doi:10.20944/preprints202306.0911.v1



## Appendix A

*Appendix A.1*

**Table A1.** Stability range of vortex states for each value of the mean free path studied. Second critical field is included in the last column.

| $l/nm$ | $1st/mT$ | $2nd/mT$ | $3rd/mT$ | $4th/mT$ | $5th/mT$ | $6th/mT$ | $7th/mT$ | $8th/mT$ | $H_2/mT$ |
|---|---|---|---|---|---|---|---|---|---|
| 0.2 | 27.29 | | | | | | | | 49.69 |
| 0.3 | 32.09 | | | | | | | | 59.29 |
| 0.4 | 36.89 | 68,89 | | | | | | | 91.28 |
| 0.5 | 36.89 | 68,29 | | | | | | | 94.48 |
| 0.6 | 38,49 | 70,49 | 97.68 | | | | | | 107.28 |
| 0.7 | 40,09 | 73,69 | 99.28 | | | | | | 118.48 |
| 0.8 | 41,69 | 75,29 | 102.48 | | | | | | 128.08 |
| 0.9 | 43,29 | 76,89 | 104.08 | | | | | | 140.88 |
| 1.0 | 44,89 | 78,49 | 105.68 | | | | | | 147.28 |
| 1.1 | 44,89 | 80,09 | 107.28 | 132.88 | | | | | 177.67 |
| 1.2 | 46,49 | 81,68 | 110.48 | 134.48 | 155.28 | | | | 177.67 |
| 1.3 | 48,09 | 84,88 | 112.08 | 136.08 | 156.88 | | | | 188.87 |
| 1.4 | 49,69 | 84,88 | 113.68 | 137.68 | 158.48 | | | | 198.47 |
| 1.5 | 49,69 | 86,48 | 115.28 | 140.88 | 161.68 | 179.27 | | | 208.07 |
| 1.6 | 51,29 | 86,48 | 116.88 | 142.48 | 163.28 | 182.47 | | | 217.67 |
| 1.7 | 52,89 | 88,08 | 118.48 | 144.08 | 164.87 | 184.07 | 203.27 | | 233.67 |
| 1.8 | 52,89 | 88,08 | 118.48 | 145.68 | 166.47 | 185.67 | 206.47 | | 241.67 |
| 1.9 | 54,49 | 89,68 | 120.08 | 147.28 | 168.07 | 187.27 | 208.07 | 227.27 | 264.06 |
| 2.0 | 54,49 | 89,68 | 121.68 | 147.27 | 169.67 | 188.87 | 211.27 | 228.80 | 265.66 |

* Tables may have a footer.

## Appendix B

Fig. A1 shows the modification of the mean free path in selected zones of Pb island, which is totally possible using nanopattering Ion technique [25–27].

Preprints (www.preprints.org) | NOT PEER-REVIEWED | Posted: 13 June 2023 doi:10.20944/preprints202306.0911.v1



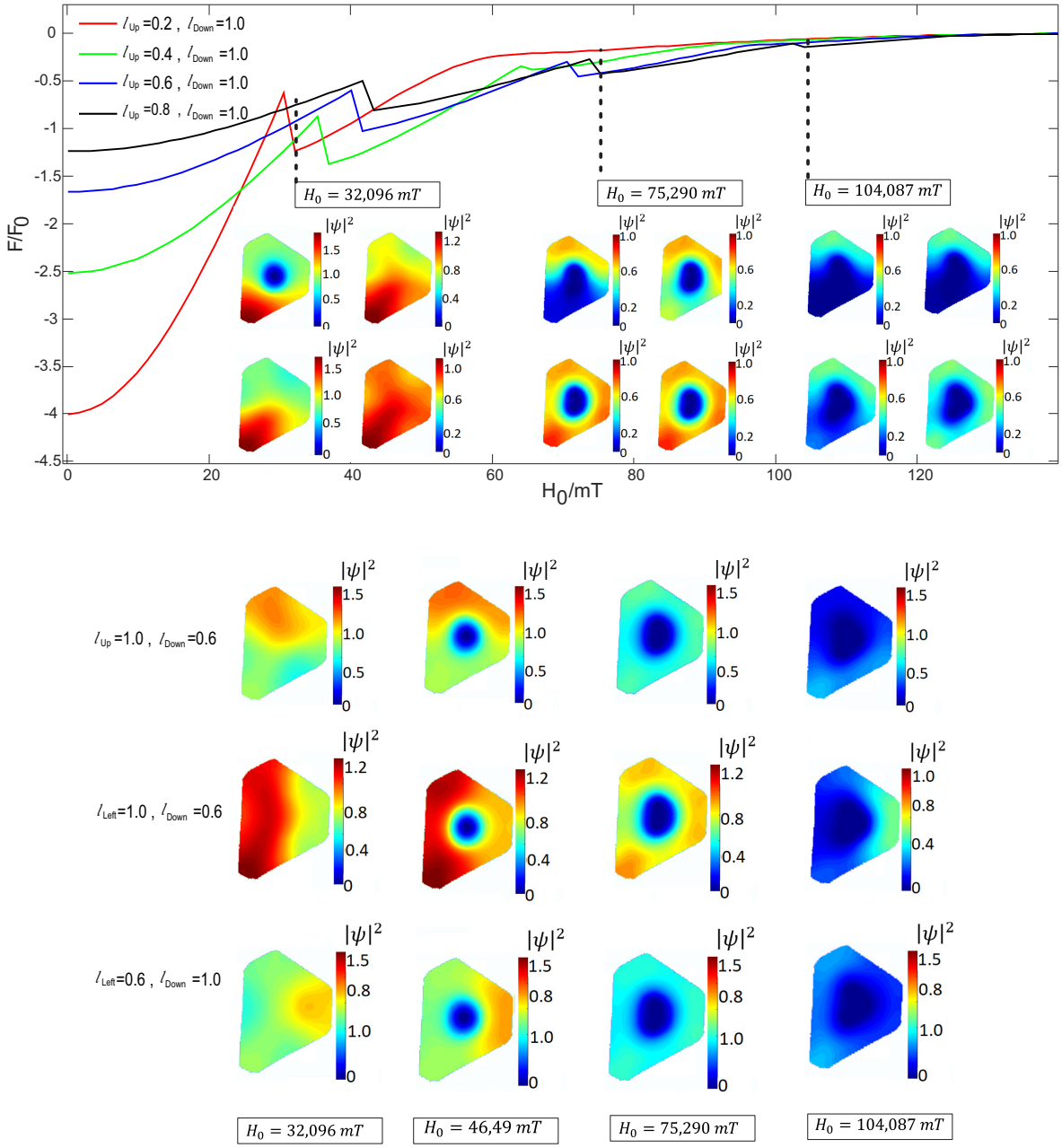


**Figure A1.** The figure shows the free energy as a function of the applied magnetic field. $l_{up}$ and $l_{down}$ show the values of mean free path at the top and bottom respectively, while $l_{left}$ shows $l_{rigth}$ for the left and right zones. Inside the figure we can see the clear modification of the vortex input under the influence of the mean free path, which implies a greater control of the superconducting condensate and the vortex configuration.

## References


1. Tinkham, M.*Introduction to Superconductivity, 2nd ed.*;Dover Publications, Inc. : New York, USA, 2004.
2. Moshchalkov, V. V.; Qiu, X. G.; Bruyndoncx, V. Paramagnetic Meissner effect from the self-consistent solution of the Ginzburg-Landau equations. *Phys. Rev. B* **1997**, *55*, 173.
3. Schweigert, V. A.; Peeters, F. M.; Singha Deo P. Vortex Phase Diagram for Mesoscopic Superconducting Disks. *Phys. Rev. Lett.* **1998**, *81*, 2783.
4. Mel'nikov, A .S.; Ryzhov, D. A.; Silaev, M. A. Electronic structure and heat transport of multivortex configurations in mesoscopic superconductors. *Phys. Rev. B.* **2008**, *78*, 064513.
5. Geim, A. K.;Grigorieva, I. V.;Dubonos, S. V.;Lok, J. G. S.; Maan, J. C.; Filippov, A. E.; Peeters, F. M. Phase transitions in individual sub-micrometre superconductors. *Nature* **1997**, *390*, 259.
6. V. A. Schweigert and F. M. Peeters Flux Penetration and Expulsion in Thin Superconducting Disks. *Phys. Rev. Lett.* **1999**, *83*, 2409.

7. Gonzáleza, J.D.; Joya, M.R.;Barba-Ortega, J. Flux Vortex state in thermally-induced pinning patterns in superconducting film. *Phys. Lett. A.* **2018**, *382*, 3103–3108.
8. Gonzáleza, J.D.; Gaona, O.J.;Barba-Ortega, J. Flux Vortex state in thermally-induced pinning patterns in superconducting film. *J. Low Temp. Phys.* **2020**, *198*, 123-134.
9. Milošević, M.; Peeters, F. M. Vortex manipulation in a superconducting matrix with view on applications. *Appl. Phys. Lett.* **2010**, *96*, 192501.
10. Berdiyorov, G. R.; Baelus, B. J.; Milošević, M. V.; Peeters, F. M. Stability and transition between vortex configurations in square mesoscopic samples with antidots. *Phys. Rev. B* **2003**, *68*, 174521.
11. Berdiyorov, G. R.; Baelus, B. J.; Milošević, M. V.; Peeters, F. M. The superconducting state in square mesoscopic samples with two and four antidots. *Physica C:Superconductivity* **2004**, *404*, 1-4.
12. Jelić, Ž. L.; Milošević, M. V.; Silhanek, A. V. Velocimetry of superconducting vortices based on stroboscopic resonances. *Sci Rep* **2016**, *6*, 35687.
13. Little, W. A.; Parks,R. D. Observation of Quantum Periodicity in the Transition Temperature of a Superconducting Cylinder. *Phys. Rev. Lett.* **1962**, *9*, 9.
14. Boato, G.; Gallinaro G.; Rizzuto C. Direct evidence for quantized flux threads in type - II superconductors. *Solid State Communications* **1962**, *3*, 173-176.
15. Moshchalkov, V.V.; Gielen, L.; Strunk, C.; Jonckheere, R.; Qiu, X.; Van Haesendonck, C.; Bruynseraede, Y. Effect of sample topology on the critical fields of mesoscopic superconductors. *nature* **1995**, *373*, 319-322.
16. Nishio, T. et al. Scanning Hall probe microscopy of vortex patterns in a superconducting microsquare. *Phys. Rev. B.* **2008**, *77*, 012502.
17. Kanda, A.; Baelus, B. J., Peeters, F. M.; Kadowaki, K.; Ootuka, Y. Experimental Evidence for Giant Vortex States in a Mesoscopic Superconducting Disk. *Phys. Rev. Lett.* **2004**, *93*, 257002.
18. Nishio, T. et al. Superconductivity of nanometer-size Pb islands studied by low-temperature scanning tunneling microscopy. *Appl. Phys. Lett.* **2006**, *88*, 113115.
19. Okayasu, S. et al. Vortex imaging in microscopic superconductors with a scanning SQUID microscope. *IEEE Transactions on Applied Superconductivity* **2005**, *15*, 696-698.
20. Karapetrov, G.;Fedor, J.; Iavarone, M.; Rosenmann, D.; Kwok, W. K. Vortex imaging in microscopic superconductors with a scanning SQUID microscope. *Phys. Rev. Lett.* **2005**, *95*, 167002.
21. Cren, T.; Fokin, D.; Debontridder, F.; Dubost, V.; Roditchev, D. Ultimate Vortex Confinement Studied by Scanning Tunneling Spectroscopy. *Phys. Rev. Lett.* **2009**, *102*, 127005.
22. Nishio, T. et al. D. Superconducting Pb Island Nanostructures Studied by Scanning Tunneling Microscopy and Spectroscopy. *Phys. Rev. Lett.* **2008**, *101*, 167001.
23. Roditchev, D.; Brun, C.; Sierrer-Garcia, L.; Cuevas, J.; Liola, V.; Milošević, M.; Debontridder, F.; Stolyarov, V.; Cren, T. Direct observation of Josephson vortex cores. *Nature* **2015**, *11*, 332–337.
24. Miller, J.H., Jr.; Villagrán, M.Y.S. Time-Correlated Vortex Tunneling in Layered Superconductors. *Condens. Matter* **2017**, *2*, 21.
25. Orús, P.; Córdoba, R.; De Teresa, J.M. *Nanofabrication: Nanolithography techniques and their applications*, 1st ed.; IOP Publishing, United Kindom, 2020.
26. Utlaut, M. *Focused ion beams for nano-machining and imaging*, 1st ed.; Woodhead Publishing, USA, 2014.
27. Orús, P.; Sigloch, F.; Sangiao, S.; De Teresa, J.M. Superconducting Materials and Devices Grown by Focused Ion and Electron Beam Induced Deposition. *Nanomaterials* **2022**, *12*, 1367.
28. Geahel, M.; Jouanny, I.; Gorse-Pomonti, D.; Poirier-Quinot, M.; Briatico, J.; Van der Beek, C.J.Edge Contamination, Bulk Disorder, Flux Front Roughening, and Multiscaling in Type II Superconducting Thin Films. *Condens. Matter* **2017**, *2*, 27.
29. Maccari, I.; Benfatto, L.; Castellani, C. Uniformly Frustrated XY Model: Strengthening of the Vortex Lattice by Intrinsic Disorder. *Condens. Matter* **2021**, *6*, 42.
30. Chong, S. V. et al. Surface superconductivity on $SrFe_2As_2$ single crystals induced by ion implantation. *EPL* **2011**, *94*, 37009.
31. Koren, G. Magnetoresistance, Gating and Proximity Effects in Ultrathin NbN-$Bi_2Se_3$ Bilayers. *Condens. Matter* **2017**, *2*, 14.
32. Fagaly, R. L. Superconducting quantum interference device instruments and applications. *Review of Scientific Instruments* **2006**, *77*, 101101.
33. Natarajan, C. M., Tanner, M. G., Hadfield, R. H. Superconducting nanowire single-photon detectors: physics and applications. *Superconductor science and technology* **2012**, *25*, 063001.
34. Vion, D.; Aassime, A.; Cottet, A.; Joyez, P.; Pothier, H.; Urbina, C.; Esteve, D.; Devoret, M. H. Manipulating the Quantum State of an Electrical Circuit. *Science* **2002**, *296*, 886-889.
35. Chiorescu, I.; Nakamura, Y.; Harmans, C.M.; Mooij, J. Coherent Quantum Dynamics of a Superconducting Flux Qubit. *Science* **2003**, *299*, 1869-1871.
36. Bean, C.P.; Livingston, J.D. Surface Barrier in Type-II Superconductors. *Phys. Rev. Lett.* **1964**, *12*, 14.